Bounding surface constitutive model for unsaturated soils considering microscopic pore structure and bonding effect

Bowen Han[2], *Guoqing* Cai[1,2*], *Lin* Xie[3], *Jian* Li[1,2], and *Chenggang* Zhao[1,2]

[1] Beijing Jiaotong University, Key Laboratory of Urban Underground Engineering of Ministry of Education, 100044 Beijing, China
[2] Beijing Jiaotong University, School of Civil Engineering and Architecture, 100044 Beijing, China
[3] Henan Provincial Department of Transportation, 450018 Zhengzhou, China

Abstract. This article presents a bounding surface model for unsaturated soils by using skeleton stress and bonding variable based on microcosmic pore structure as constitutive variables. A Hydraulic hysteresis soil-water characteristic curve model considering deformation and hydraulic hysteresis is combined to achieve hydraulic coupling. The proposed model can capture the change of the inter-particles bonding effect in the deformation process of unsaturated soils and accurately predict the hydraulic mechanical behavior of unsaturated soils under complicated loading paths and wetting-drying cycles. The validity of the proposed model is confirmed by the results of unsaturated isotropic compression tests, wetting-drying cycles tests and unsaturated triaxial shear tests reported in the literature.

Introduction

Unsaturated soil has a bonding effect due to the existence of water meniscus between particles, which makes the mechanical properties of unsaturated soils more complicated than saturated soils. It is of great value to establish unsaturated constitutive models considering the bonding effect. The bonding effect is related to suction, degree of saturation, and pore structure. Some researchers indirectly describe the bonding effect by considering the influence of suction and saturation in their model [1-6]. Gallipoli et al [7] were the first to establish an elastic-plastic constitutive model that directly describes the bonding effect of unsaturated soils by using a bonding variable to replace the suction.

Besides suction and degree of saturation, the effect of microscopic pore structure on the hydraulic properties of unsaturated soils are not negligible. Some researchers [8-10] found that the pore structure of unsaturated soils has a significant influence on the bonding effect and hydraulic mechanical behavior between particles. But the existing models have little consideration for the effect of microscopic pore structure. In addtiton, compared with the traditional elasto-plastic model, the bounding surface model [11] is versatile and can more accurately predict the mechanical behavior of various soil types [12-13]. For unsaturated soils with more complicated mechanical properties, it is more suitable to use the bounding surface plastic model [14-15].

In this paper, a hydraulic coupling bounding surface model for unsaturated soils using improved average skeleton stress and bonding variable as basic constitutive variables is established. Experimental results of isotropic compression tests, wetting-drying cycles tests and triaxial shear tests are used to validity the model.

2 Framework of Model

2.1 Constitutive Variables of Model

The improved average skeleton stress and bonding variable are used as the constitutive variables of the model in this paper to consider the influence of microscopic pore structure and bonding effect. Based on the research results of Alonso et al [16], the parameter χ of Bishop effective stress [17] is replaced by the effective degree of saturation S_e. The improved average skeleton stress is written as follows:

$$p^* = p_{net} + S_e s \tag{1}$$

Where p_{net} is the net stress, S_{e} is the effective degree of saturation that can be express as

$$S_e = \frac{S_r - S_{res}}{1 - S_{res}} \tag{2}$$

Where S_r is the degree of saturation, S_{res} is the residual degree of saturation

The degree of saturation S_r of the bonding variable defined by Gallipoli et al is replaced by the effective degree of saturation S_e to establish a new bonding variable as follows :

$$\zeta = f(s)(1 - S_e) \tag{3}$$

Where the $f(s)$ is the ratio of the stabilising inter-particle force at the two suctions of s and zero for the ideal case of a water meniscus located at the contact between two identical spheres; $(1-S_e)$ is the accounts for the number of water menisci between the macropores per unit volume of solid fraction.

2.2 Unsaturated Normally Consolidated Lines

Establishing the relationship between unsaturated soil deformation and bonding variable is important to determine the normally consolidated lines for unsaturated soils. Using a methodology similar to Gallipoli et al [7], the authors assume that a unique functional relationship is satisfied between e/e_s and ζ :

$$\frac{e}{e_s}=\varphi(\zeta)=1-a\left[1-\exp(b\zeta)\right] \tag{4}$$

Where e and e_s are the void ratio corresponding to the unsaturated and saturated at the same value of improved average skeleton stress p^*, a and b are fitting parameters, e_s can be calculated according to the saturated normal compression line:

$$e_s\left(p^*\right)=N-\lambda\ln p^* \tag{5}$$

Where N is the void ratio corresponding to $p^*=1$; λ is the slope of the saturated normal compression line in the $\ln p^*-e_s$ plane.

Thus, the unsaturated normal compression curve in the $\ln p^*-e_s$ plane can be calculated by combining Eq. (4) and Eq. (5) as follows:

$$e\left(p^*,\zeta\right)=\varphi(\zeta)e_s\left(p^*\right) \tag{6}$$

2.3 Yield equation

Eq. (6) defines a normal compression surface in the $\ln p^*-e-\zeta$ space. The irreversible volumetric strains occur when the stress path on the normal compression. Yield equation can be express as follows according to Hu et al [18]

$$p_c^*(\zeta)=\exp\left\{\frac{(\lambda-\kappa)\ln p_c^*(0)+N\left[\varphi(\zeta)-1\right]}{\varphi(\zeta)\lambda-\kappa}\right\} \tag{7}$$

2.4 Bounding surface

The yield surface of Modified Cam-clay model [19] is used to be the bounding surface in the proposed model. Fig. 1 shows the bounding surface in three-dimensional state, the bounding surface can be expressed as follows:

$$F=\overline{q}^2-M\ \overline{p}^*\left\{\overline{p}_c^*\left[\zeta,p_c^*(0)\right]-\overline{p}^*\right\}=0 \tag{8}$$

Where $\overline{p}^*$ is the improved average skeleton stress on the bounding surface, $\overline{q}$ is the deviator stress on the bounding surface, $\overline{p}_c^*[\zeta,\ p_c^*(0)]$ is the yield stress corresponding to constant value of bonding variable ζ defined by Eq. (7) , M is the slope of the critical state line.

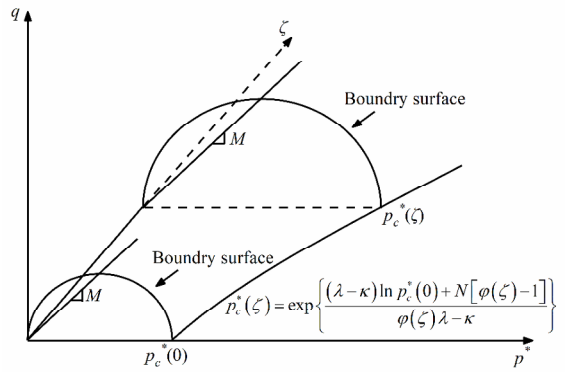

Fig. 1. Bounding surface in the $p^*-q-\zeta$ space

2.5 Flow rule

A non-associated flow rule is chosen in the proposed model. The plastic potential surface equation is written as follows:

$$g=\alpha\overline{q}^2-M\ \overline{p}^*\left\{\overline{p}_c^*\left[\zeta,p_c^*(0)\right]-\overline{p}^*\right\}=0 \tag{9}$$

Where α is a parameter determined by zero lateral strain when the stress state corresponds to the K_0 value [20], according to the derivation of Alonso et al [1], α can be expressed as

$$\alpha=\frac{\lambda}{\lambda-\kappa}\frac{M(M-9)(M-3)}{9(6-M)} \tag{10}$$

The incremental forms of plastic strain and plastic shear strain can be obtained as follows:

$$\begin{cases}d\varepsilon_v^p=\Lambda\dfrac{\partial g}{\partial\overline{p}^*}\\ d\varepsilon_s^p=\Lambda\dfrac{\partial g}{\partial\overline{q}}\end{cases} \tag{11}$$

Where Λ is the plastic multiplier.

According to the plastic theory of bounding surface, plastic multiplier Λ can be expressed as follows:

$$\Lambda=\frac{1}{\overline{K}_p}\left(\frac{\partial F}{\partial\overline{p}^*}d\overline{p}^*+\frac{\partial F}{\partial\overline{q}}d\overline{q}\right) \tag{12}$$

Where $\overline{K}_p$ is the plastic modulus corresponding to the mapping point on the bounding surface.

2.6 Hardening law

The yield stress $p_c^*(0)$ is chosen as the hardening parameter of the proposed model. The hardening law can be obtained as follows:

$$\frac{dp_c^*(0)}{p_c^*(0)}=\frac{1+e}{\lambda-\kappa}d\varepsilon_v^p \tag{13}$$

Where $d\varepsilon_v^p$ is the plastic volumetric strain increment.

The plastic modulus on the bounding surface can be obtained by combining the flow rule, hardening law and the condition of consistency on the bounding surface.

2.7 Mapping rule

Zienkiewicz et al [21] establishes radial mapping rules with simple form, few parameters, and good applicability. A similar radial mapping rule is used in the proposed model:

$$K_p = \bar{K}_p \left(\frac{\delta_0}{\delta} \right)^r \tag{14}$$

where δ is the distance between the current stress point and the mapping origin, δ_0 is the distance between the mapping point and the mapping origin, r is the mapping exponent related to the basic physical properties of the soils:

$$r = r_0 \exp\left(-n \int \left| d\varepsilon^{\mathrm{p}} \right| \right) \tag{15}$$

where r_0 is an initial value, n is proportionally constant ($n > 0$), $\int \left| d\varepsilon^{\mathrm{p}} \right|$ is cumulative value of plastic strain increment.

As shown in Fig. 2, the mapping origin is the coordinate origin in the $p^* - q$ plane, and the mapping point on the bounding surface is determined by the intersection of the line connecting the mapping origin to the current stress point and the bounding surface.

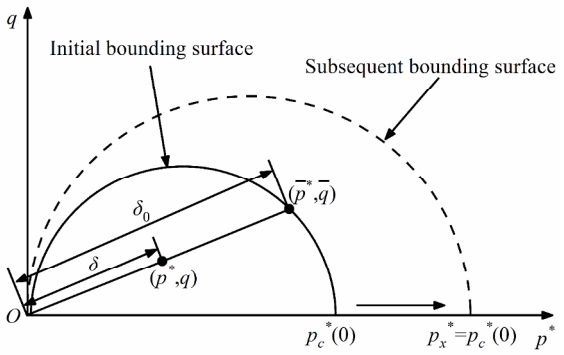

Fig. 2. Mapping rule.

The elastic volumetric strain increment and the elastic shear strain increment can be calculated as follows:

$$\begin{cases} d\varepsilon_v^e = \dfrac{\kappa}{1+e} \dfrac{dp^*}{p^*} \\ d\varepsilon_s^e = \dfrac{dq}{3G} \end{cases} \tag{16}$$

where G is elastic shear modulus.

2.8 Hydraulic behaviour

Gallipoli et al [22] developed a soil-water characteristic curve model considering deformation effect based on the van Genuchten model [23], which is very representive:

$$S_r = \left\{ 1 + \left[m_1 (v-1)^{m_2} s \right]^{m_3} \right\}^{-m_4} \tag{17}$$

Where v is specific volume, m_1, m_2, m_3 m_4 are fitting parameters.

Based on Gallipoli et al [22], the authors establish a soil-water characteristic curve model considering hydraulic hysteresis to achieve hydraulic coupling. The main drying curve and the main wetting curve are defined as follows:

$$\begin{cases} S_{ed} = \left\{ 1 + \left[m_{1d} (v-1)^{m_2} s \right]^{m_3} \right\}^{-m_4} \\ S_{ew} = \left\{ 1 + \left[m_{1w} (v-1)^{m_2} s \right]^{m_3} \right\}^{-m_4} \end{cases} \tag{18}$$

Where m_{1d} is fitting parameters for the main drying curve, m_{1w} is fitting parameters for the main wetting curve.

The scanning curve equations are expressed as follow based on Zhou et al [6]

$$\frac{\partial S_{es}}{\partial s} = \begin{cases} \left(\dfrac{s_d}{s} \right)^{-\eta} \left(\dfrac{\partial S_{ed}}{\partial s} \right) & s_d = \dfrac{\left(S_e^{-1/m_4} - 1 \right)^{1/m_3}}{m_{1d} (v-1)^{m_2}} \\ \left(\dfrac{s_w}{s} \right)^{\eta} \left(\dfrac{\partial S_{ew}}{\partial s} \right) & s_w = \dfrac{\left(S_e^{-1/m_4} - 1 \right)^{1/m_3}}{m_{1w} (v-1)^{m_2}} \end{cases} \tag{19}$$

where S_{ed} is the effective degree of saturation corresponding to the main drying curve, S_{ew} is the effective degree of saturation corresponding to the main wetting curve, s_d is the suction corresponding to the main drying curve at the same effective degree of saturation as the current point in the s–S_e plane, s_w is the suction corresponding to the main wetting curve at the same effective degree of saturation as the current point in the s–S_e plane, η is the parameter that controls the shape of the scanning curves.

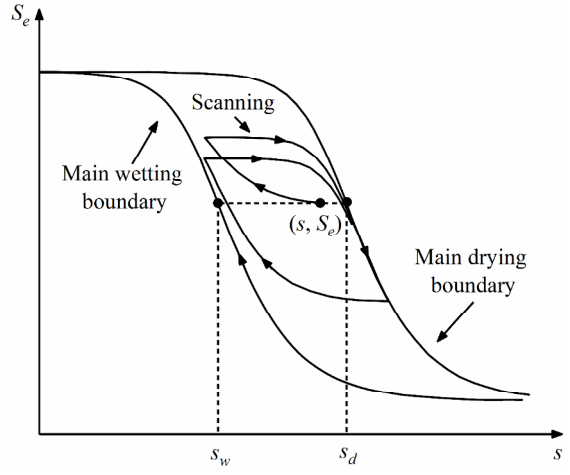

Fig. 3. Scanning curve diagram.

Fig. 3 shows the scanning curve diagram. The incremental forms of effective degree of saturation during drying and wetting process are obtained as follows:

$$\begin{cases} dS_{ed} = \dfrac{\partial S_{eds}}{\partial s} ds + \dfrac{\partial S_{ed}}{\partial v} dv \\ dS_{ew} = \dfrac{\partial S_{ews}}{\partial s} ds + \dfrac{\partial S_{ew}}{\partial v} dv \end{cases} \tag{20}$$

Where S_{eds} is the effective degree of saturation corresponding to the drying scanning curve, S_{ews} is the effective degree of saturation corresponding to the wetting scanning curve.

3 Model verification

A series of experimental data of reconstituted kaolin [24], mixture of bentonite and kaolin [25] are used to verify the prediction results of the proposed model. The predictions include: (a) isotropic compression tests at constant suction; (b) wetting-drying cycle tests at constant net stress; (c) triaxial shear tests at constant suction. The parameters of reconstituted kaolin are: N=1.64, λ=0.128, κ=0.02, $p_c^*(0)$=18 kPa, M=0.73, G=10000 kPa, a=0.359, b=1.286, r_0=5, n=1, S_{res}=0.05. The parameters of mixture of bentonite and kaolin are: N=1.759, λ=0.144, κ=0.04, $p_c^*(0)$=17 kPa, a=0.349, b=1.366, r_0=5, n=10, m_{1w}=0.0195, m_{1d}=0.0047, m_2=6.911, m_3=3.929, m_4=0.03636, η=0.45, S_{res}=0.05. Fig. 3, Fig. 4, Fig. 5 show the comparisons between model predictions and experimental data.

3.1 Isotropic compression tests at constant suction

Sivakumar [24] conducted a series of isotropic compression tests of reconstituted kaolin at constant suctions. Two sets of tests at suctions of 200 kPa, and 300 kPa are used to verify the proposed model. The isotropic loading paths experienced by the samples under each suction is 50 kPa→200 kPa, 50 kPa→250 kPa.

Fig. 4 shows the comparisons between model predictions and experimental data. The model can accurately predict the variation of void ratio. As the net stress increases, the void ratio gradually decreases.

3.2 Wetting-drying cycle test at constant net stress

The experiment results of constant net stress wetting-drying cycle tests conducted by Sharma [25] are used to verify the performance of the proposed model. The suction path is 300 kPa→20 kPa→300 kPa.

Fig. 5 shows the comparisons between experimental results and model predictions during wetting-drying cycle. It can be seen that the proposed model can effectively capture the hydraulic hysteresis characteristics of unsaturated soils during wetting-drying cycle.

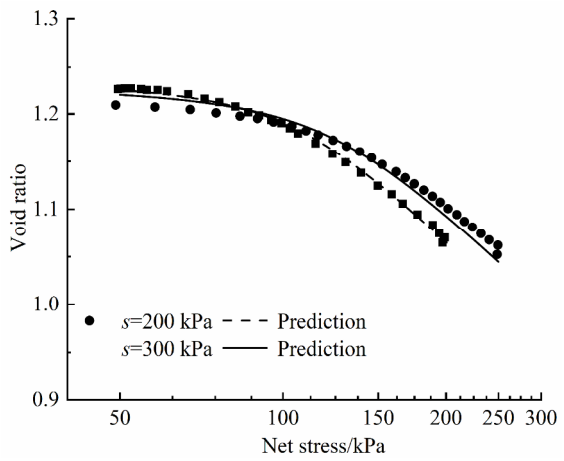

Fig. 4. Experimental results and model predictions for constant suction isotropic compression tests.

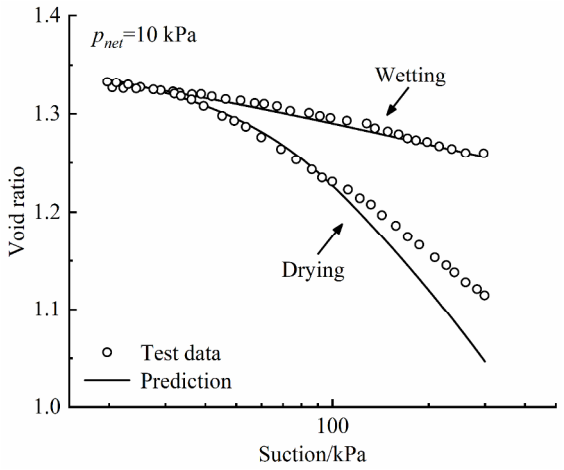

Fig. 5. Experimental results and model predictions for constant net stress wetting-drying cycle test.

3.3 Triaxial shear tests at constant suction

Sivakumar [25] conducted a series of triaxial shear tests on reconstituted kaolin at the suctions of 200 kPa, 300 kPa. The samples first experience a consolidation with a net stress path of 50 kPa→100 kPa and then maintain the stress path of $\Delta q/\Delta p_{net}$=3 for drainage shearing.

The comparisons between experimental results and model predictions of constant suction triaxial shear tests are shown in Fig. 6. Clearly the proposed model can effectively predict the mechanical behavior of unsaturated soil experiencing triaxial shearing. The deviator stress increase with the increase of the axial strain, the specific volume decrease with the increase of the axial strain, finally reaches the critical state. As the suction increases, the deviator stress increases gradually.

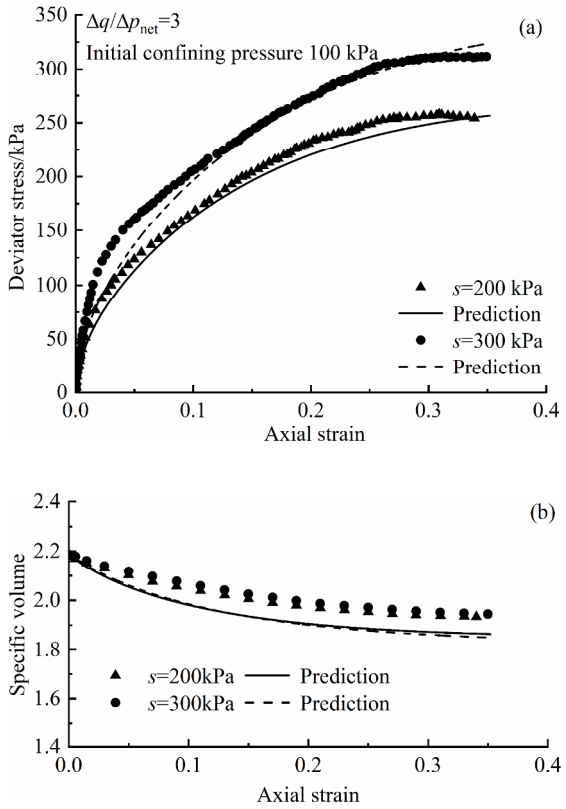

Fig. 6. Experimental results and model predictions for constant suction triaxial shear tests. (a) axial strain-deviator stress; (b) axial strain-specific volume.

4 Conclusions

A new hydraulic coupling bounding surface model for unsaturated soils considering microscopic pore structure and bonding effect is established in this article. Using the effective degree of saturation to replace the degree of saturation, a new average skeleton stress and bonding variable are established as the constitutive variables of the model, the plastic deformation is calculated by the bounding surface plasticity theory, and the hydraulic coupling is achieved by combining the hydraulic hysteresis soil-water characteristic curve model considering the influence of deformation. The proposed model can effectively predict the mechanical behavior of unsaturated soils under isotropic loading, shear loading and wetting-drying paths.

Acknowledgements

This research was financially supported by the National Natural Science Foundation of China (51722802, U1834206), Beijing Municipal Natural Science Foundation (8202038)，Beijing Nova Program (Z181100006218005), and the Research Funds of Henan Provincial Department of Transportation (2017B4).

References

1. E. E. Alonso, Gens. A, A. Josa. Géotechnique. **40**, 405 (1990).
2. G. Bolzon, B. A. Schrefler, O. C. Zienkiewicz. Géotechnique. **46**, 279 (1996).
3. Y. J. Cui, and P. Delage. Géotechnique. **46**, 291 (1996).
4. S. J. Wheeler, R. S. Sharma, M. S. R. Buisson. Géotechnique. **53**, 41 (2003).
5. D. C. Sheng, S. W. Sloan, A. Gens. Comput. Mech. 2004, **33**, 453 (2004).
6. A. N. Zhou, D. C. Sheng, S. W. Sloan, A. Gens. Comput. Geotech. **43**, 178 (2012).
7. D. Gallipoli, A. Gens, R. S. Sharma, J. Vaunat, Géotechnique. **53**, 123 (2003).
8. E, Romero, A. Gens, A. Lloret. Eng. Geol. **54**, 117 (1999).
9. C. Hoffmann, E. E. Alonso, E. Romero. Phys. Chem. Earth. **32**, 832 (2007).
10. E. E. Alonso, E. Romero, C. Hoffmann. Géotechnique. **61**, 329 (2011).
11. Y. F. Dafalias. J. Eng. Mech. **112**, 966 (1986).
12. R. S. Crouch, J. P. Wolf, Y. F. Dafalias. J. Eng. Mech. **120**, 2251 (1994).
13. C. Hu, H. Liu, W. Huang. Comput. Geotech. **44**, 34 (2012).
14. A. R. Russell, N. Khalili. Int. J. Numer. Anal. Methods. Geomech. **30**, 181 (2006).
15. D. Masin. Int. J. Numer. Anal. Meth. Geomech. **34**, 73 (2010).
16. E. E. Alonso, J. M. Pereira, J. Vaunat, S. Olivella. Géotechnique. **62**, 463 (2010).
17. A. W. Bishop. *Teknisk Ukeblad* **106**, 859 (1959).
18. R. Hu, H. H. Liu, Y. F. Chen, C. B. Zhou, D. Gallipoli. Comput. Geotech. **59**, 127 (2014).
19. K. H. Roscoe, J. B. Burland. Eng. Plast. **3**, 539 (1968).
20. J. Jaky. *Proc 2nd Int. Conf. Soil. Mech and Fdn Engng, Rotterdam*, **1**, 103 (1948).
21. O. C. Zienkiewicz, K. H. Leung, M. Pastor. Simple model for transient soil loading in earthquake analysis. I. Basic model and its application. Int. J. Numer. Anal. Methods. Geomech. **9**, 453 (1985).
22. D. Gallipoli, S. J. Wheeler, M. Karstunen. Géotechnique. **53**, 105 (2003).
23. M. T. Van Genuchten. Soil. Sci. Soc. Am. J. **44**, 892 (1980).
24. V. Sivakumar. Ph.D. thesis, Univ. of Sheffield, Sheffield, U.K. (1993).
25. R. S. Sharma. Ph.D. thesis, Univ. of Oxford, Oxford, U.K. (1998).